

Enhanced Charge Injection in Pentacene Field-Effect Transistors with Graphene Electrodes

Sangchul Lee, Gunho Jo, Seok-Ju Kang, Gunuk Wang, Minhyeok Choe, Woojin Park, Dong-Yu Kim, Yung Ho Kahng,* and Takhee Lee*

Organic electronic devices have generated a great deal of research interest because of their low-cost fabrication, limitless material variety, and the myriad of potential applications.^[1–9] Significant research efforts have been directed towards improving the performance of devices such as organic field-effect transistors (OFETs).^[4–9] One important approach for improving this performance is to select contact-electrode materials that yield efficient charge injection into the active channels.^[7–9] Contact electrodes affect the device performance by determining the carrier type from the energy-level alignment and by governing charge injection, which is related to the quality of the contacting interface.^[10,11] Noble metals and doped metal-oxide films have conventionally been used as electrode materials. However, problems with metal-oxide films include their inflexibility and high cost.^[12] In addition, Au, which is predominantly used as an electrode in OFETs, has shown a significant charge-injection barrier because of unfavorable interface dipole layer formation.^[13,14] Therefore, alternative electrode materials must be found to avoid such shortfalls.^[7–9,15–17]

Recently, graphene-based thin films have attracted great attention as an alternative electrode material for organic electronic devices.^[18] Graphene, a two-dimensional conducting sheet, is transparent and conducting and has good mechanical stability and flexibility.^[19,20] Large samples of multilayer graphene (MLG) films have been synthesized by chemical vapor deposition (CVD) or solution-based methods, rendering them realistic prospects as electrodes.^[21–23] To date, MLG films have exhibited a promising performance as electrodes for many organic devices such as organic transistors,^[15–17] light-emitting diodes,^[24,25] and photovoltaics.^[26–29] However, to establish MLG films as viable alternative electrodes for organic devices and to provide fundamental engineering routes for better performances, detailed studies on the interface between the MLG film and organic materials are necessary. Because the interfacial characteristics such as contact resistance, dipole effect, and

charge injection barrier height strongly dominate the charge-injection properties, these characteristics need to be analyzed.

In this work, we report on the efficient charge injection in pentacene OFETs with graphene electrodes. Pentacene OFETs are an excellent choice to investigate the properties of the interface because they are known to be reliable, exhibit a high mobility, and have been studied for many years as organic semiconductor devices.^[30,31] We show that the OFET performance was significantly improved by using MLG electrodes; the output and transfer currents and mobility increased in comparison to conventional OFETs with Au electrodes. Detailed investigations on the contact resistance and charge-injection barrier height revealed that such improvements were a result of the superior interfacial contact between the MLG electrode and the pentacene organic channels. Our findings will aid in establishing graphene-based thin films as an efficient electrode material for improving OFETs and other types of organic electronic devices.

The fabrication process of pentacene OFETs with patterned MLG electrodes is illustrated in **Figure 1**. The graphene synthesis is explained in the Experimental section. The grown MLG film was detached from the growth substrate by using a catalyst-etching and scooping-up technique with aqueous iron chloride (FeCl₃) solution (around 1 M) as the etchant (**Figure 1a**),^[21,32] and transferred onto a 300-nm-thick SiO₂ layer on a heavily doped Si wafer (**Figure 1b**). Then, a 50-nm-thick Ni layer was evaporated through a shadow mask onto the MLG film (**Figure 1c**), and the substrate was exposed to oxygen plasma at 200 mTorr and 50 W to remove the MLG film from the unprotected regions (**Figure 1d**). The Ni mask patterns were then etched away in FeCl₃ solution (**Figure 1e**). The patterned graphene electrodes were coated with poly(methylmethacrylate) (PMMA). Subsequently, the PMMA-coated graphene electrodes were detached from the SiO₂ substrate by etching the SiO₂ layer with buffered oxide etchant. Then, the detached graphene electrodes were transferred onto an octadecyltrichlorosilane (OTS)-treated substrate. After this, the PMMA was removed by acetone. Finally, a pentacene layer (ca. 60 nm thick) was deposited using a thermal evaporator under vacuum through a shadow mask onto the patterned MLG electrodes (**Figure 1f**). The fabricated OFETs had a width of 1000 μm and channel lengths of 50, 100, 200, and 300 μm.

Figure 2 shows the typical characteristics of the graphene-electrode pentacene OFETs (denoted as GR-pentacene OFETs). Also shown are the characteristics of Au-electrode pentacene OFETs (denoted as Au-pentacene OFETs) for comparison. **Figure 2a** presents the output characteristics, that is, the drain current versus drain voltage (I_D – V_D) curves at a fixed gate voltage (V_G) of –50 V for GR-pentacene and Au-pentacene OFETs with

S. Lee, G. Jo, S.-J. Kang, G. Wang, M. Choe, W. Park,
Prof. D.-Y. Kim, Dr. Y. H. Kahng, Prof. T. Lee
Department of Nanobio Materials and Electronics
Department of Materials Science and Engineering
Gwangju Institute of Science and Technology
Gwangju 500–712, Korea
E-mail: yhkahng@gist.ac.kr; tlee@gist.ac.kr
Dr. Y. H. Kahng
Research Institute for Solar and Sustainable Energies
Gwangju Institute of Science and Technology
Gwangju 500–712, Korea

DOI: 10.1002/adma.201003165

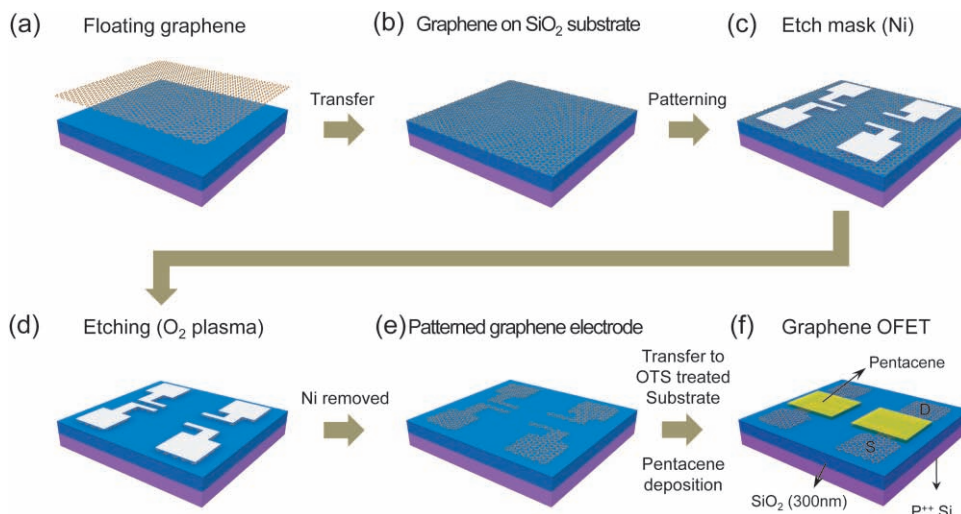


Figure 1. Fabrication process of OFETs with patterned MLG electrodes. a) The MLG film is floating after etching of the Ni substrate in FeCl_3 solution. b) The MLG film is transferred to a 300-nm-thick SiO_2 on a highly p-doped silicon substrate. c) The Ni patterns are deposited via a shadow mask. d) The MLG film is etched by exposure to oxygen plasma. e) The Ni is removed after which the electrodes are transferred to an OTS-treated substrate. f) The pentacene layer (ca. 60 nm) is deposited on the graphene electrodes to form the active layer.

a channel length of 50 μm . The inset in Figure 2a shows an optical image of a fabricated GR-pentacene OFET device. The transfer characteristics (I_D - V_G) curves at a fixed V_D of -50 V are shown in Figure 2b. It is noteworthy that the I_D is higher for the GR-pentacene OFET than for the Au-pentacene OFET at the same V_D or V_G values. These results indicate that the GR-pentacene OFET is superior to the Au-pentacene OFET, which is in agreement with other reports that have shown improved performance of graphene electrodes over conventional electrodes.^[16,17] In our study, the role of graphene electrodes as an efficient charge-injection layer to pentacene organic channels was investigated in terms of key parameters such as the contact resistance, charge-injection barrier height, and mobility.

The contact resistance (R_C) can be obtained by characterizing the device characteristics as a function of the channel length. Figure 3a and 3b show a series of I_D - V_D at a fixed V_G (-50 V) and I_D - V_G curves at a fixed V_D (-50 V), respectively, of GR-pentacene

OFETs with different channel lengths of 50, 100, 200, and 300 μm . The detailed data for GR-pentacene and Au-pentacene OFETs are provided in Figure S2 and S3 in the Supporting Information. In particular, the I_D values decreased as the channel length increased because the channel resistance generally increases with channel length. Figure 3c displays the linear dependence of the total resistance (R_{tot}) on the channel length. Here, the R_{tot} values were obtained from the slopes of the linear segments in the low- V_D region (from 0 to -1 V) of the I_D - V_D curves (Figure 3a). The R_C can be obtained as the y-intercept of the extrapolation fit of R_{tot} versus the channel length data. The R_C was determined to be around 0.56 $\text{M}\Omega$ (at a V_G of -50 V) for GR-pentacene OFETs. However, using the same characterization method, a larger R_C value (ca. 0.85 $\text{M}\Omega$) was obtained for Au-pentacene OFETs at a V_G of -50 V.

The R_C was further investigated by performing the same measurements at different V_G values (see Figure S5 in the

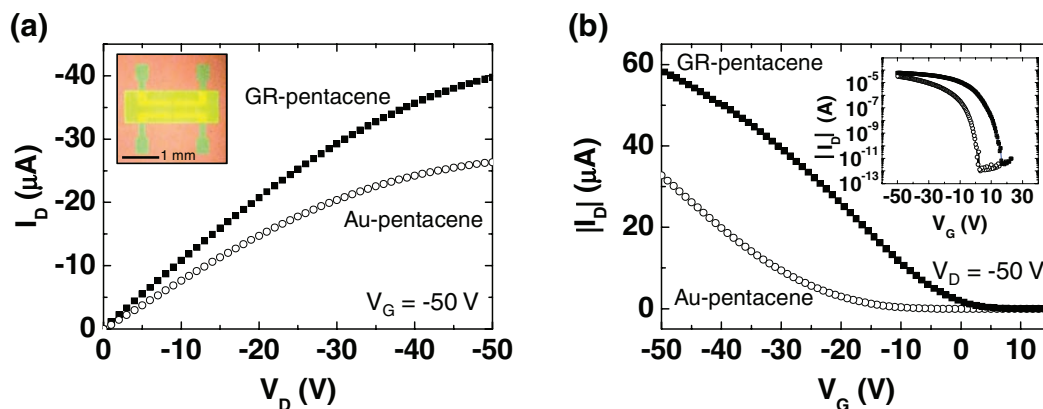


Figure 2. a) I_D - V_D and b) I_D - V_G characteristics of GR-pentacene and Au-pentacene OFETs with a channel length of 50 μm . The inset in (a) is an optical image of a fabricated GR-pentacene OFET device. The inset in (b) shows the transfer characteristics on a semi-logarithmic scale.

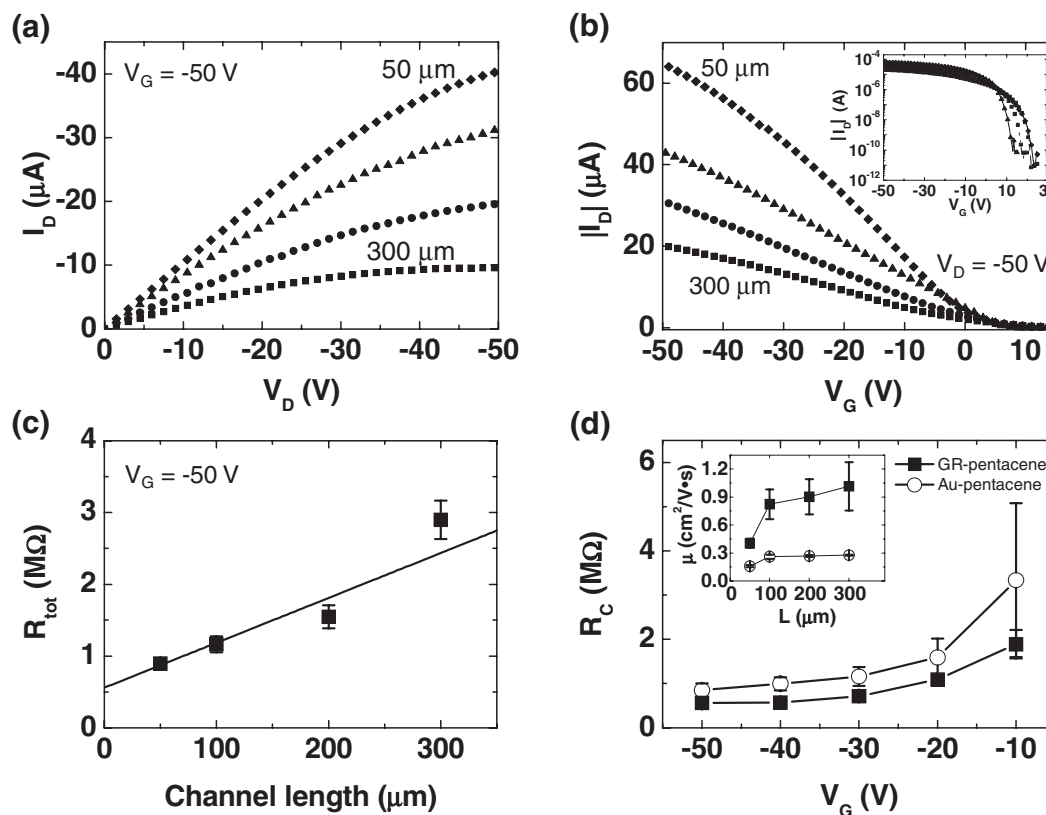


Figure 3. a) I_D - V_D characteristics for GR-pentacene OFETs with various channel length (L) of 50, 100, 200, and 300 μm at a fixed V_G of -50 V. b) I_D - V_G characteristics for GR-pentacene OFETs with various channel lengths at a fixed V_D of -50 V. c) Resistance versus channel length for GR-pentacene OFETs at a fixed V_G of -50 V. In this plot, the y -intercept is the contact resistance (R_C). d) R_C versus V_G of GR-pentacene and Au-pentacene OFETs. The error bars in (c) and (d) were obtained from measuring the standard deviation of about 7 devices for each data point. The inset in (d) compares the saturation mobility (μ) of both types of OFETs with different channel lengths at a fixed V_G of -50 V.

Supporting Information). As summarized in Figure 3d, the R_C decreased with V_G becoming more negative for both GR-pentacene and Au-pentacene OFETs. Such a decrease in R_C with more negative V_G is correlated to the higher density of charge in the conducting channel in the large channel-length regime (e.g., R_{channel} (channel resistance) $> R_C$).^[33–35] More importantly, the R_C values of GR-pentacene OFETs were found to be smaller than those for Au-pentacene OFETs at all V_G values. Furthermore, the saturation region mobilities for GR-pentacene OFETs (0.40 – 1.01 $\text{cm}^2 \text{V}^{-1} \cdot \text{s}^{-1}$) were observed to be higher than those for Au-pentacene OFETs (0.16 – 0.28 $\text{cm}^2 \text{V}^{-1} \cdot \text{s}^{-1}$), as shown in the inset of Figure 3d. Therefore, it can be concluded that the performance of pentacene OFETs is significantly improved after implementing graphene electrodes instead of conventional Au electrodes. As will be discussed below, this improvement of OFET performance originates from the improved interfacial properties of the graphene electrode and the pentacene channel.

The R_C between the electrode and the organic channel is primarily caused by the charge-injection barrier formed at the interface. Without the interfacial dipole, the hole-injection barrier (Φ_h) for p-type organic semiconductors is determined by the Schottky-Mott rule as:^[11]

$$\Phi_h = E_I - \Phi_m \quad (1)$$

where E_I is the ionization energy and Φ_m is the work function. By using Equation 1 and the known energy levels for pentacene, Au, and graphene, the expected injection barrier heights for the GR-pentacene and Au-pentacene interfaces are 0.38 and 0.1 eV, respectively (see Table S1 in the Supporting Information). This indicates that the Au electrode is expected to form better contact (lower R_C) with pentacene than the graphene electrode does. However, this prediction contradicts the experimental observation that graphene formed a better contact. Such a contradiction can be explained by considering the formation of interfacial dipoles at the interface. With an interfacial dipole, the hole-injection barrier is determined as:^[11]

$$\Phi_h = E_I - \Phi_m - \Delta \quad (2)$$

where Δ is the dipole barrier.

In fact, the effective barrier height (Φ_{eff}) can be directly measured via temperature-variable I_D - V_D characterization.^[36,37] Note that we used OFETs with a channel length of 3 μm , in which the contact resistance is more dominant for charge transport, in order to investigate the barrier height in terms of thermionic emission. If this criterion is not satisfied, then the effect of temperature on R_{ch} which has been explained by the multiple trapping and release model,^[4,38] should also be considered simultaneously. Figure 4a shows the Arrhenius plots, $\ln(I_D/T^2)$

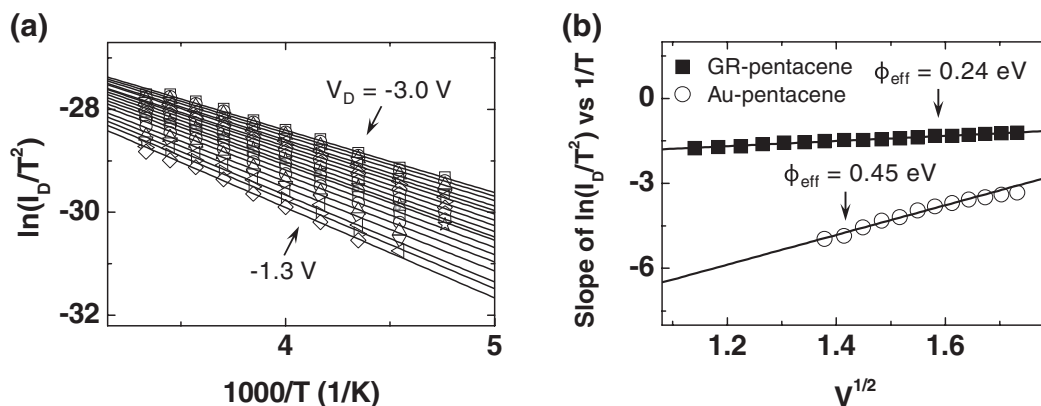


Figure 4. a) A series of plots of $\ln(I_D/T^2)$ versus $1000/T$ at various drain voltages ranging from -1.3 to -3.0 V obtained for a GR-pentacene OFET with a channel length of $3 \mu\text{m}$ and width of $100 \mu\text{m}$. b) Plots of the slopes from (a) as a function of $V_D^{1/2}$ showing a linear dependence. The y-intercept value was used to deduce the effective barrier height (Φ_{eff}). The effective barrier height from the Au-pentacene OFET is also shown for comparison.

versus $1000/T$, at various V_D ranging from -1.3 to -3.0 V for a GR-pentacene OFET with a channel length of $3 \mu\text{m}$ and width of $100 \mu\text{m}$. The observed linear dependencies in these plots are characteristic of typical thermionic emission.^[36,39] Similar characteristics were observed for the Au-pentacene OFET (see Figure S6 in the Supporting Information). The slopes of these plots are demonstrated in Figure 4b. From these plots, the barrier heights could be calculated from the y-intercepts of the linear fits of the data using the following thermionic emission equation:^[36,37,39]

$$I_D = A^* T^2 \exp\left(-\frac{q\Phi_{\text{eff}} - a\sqrt{V_D}}{k_B T}\right) \quad (3)$$

with

$$a = q \sqrt{\frac{q\Phi_{\text{eff}}}{4\pi\epsilon_0\epsilon d}} \quad (4)$$

where A^* is the effective Richardson constant, k_B is the Boltzmann constant, q is the electron charge, ϵ_0 is the permittivity of free space, ϵ is the dielectric constant of pentacene, and d is the thickness of the pentacene film.

The estimated effective barrier height using this method was around 0.24 eV for GR-pentacene OFETs and was significantly lower than that (ca. 0.45 eV) for Au-pentacene OFETs. Therefore, it can be concluded that a better contact was formed for GR-pentacene than for Au-pentacene because of the favorable orientation of the interfacial dipoles at the GR-pentacene interface, which resulted in a lowering of the hole-injection barrier. It is known that organic/organic interfaces form a small interfacial dipole that induces a lower barrier for carrier injection as compared to metal/organic interfaces.^[11,15] Accordingly, the graphene-pentacene interface forms a small and favorably oriented interfacial dipole layer, unlike the Au-pentacene interface which forms a significant interfacial dipole layer and results in a higher carrier-injection barrier.^[13,14] In addition, graphene is expected to induce a strong interaction with pentacene and to form excellent interfacial contact because it has a similar molecular structure.^[16] These findings enhance our understanding of the reason for the improved performance of graphene electrodes in the pentacene OFETs.

The effect of interfacial dipoles (Equation 2) was verified by Kelvin-probe measurements (see Table S1 in the Supporting Information). To measure the work-function changes induced by a pentacene layer on Au and graphene films, a 5-nm-thick pentacene layer was deposited on Au and graphene sheets, and the work-function changes were monitored before and after the pentacene deposition. After deposition, the work functions of the Au and graphene films changed to 4.46 and 4.71 eV from 4.90 and 4.62 eV, respectively. Therefore, the Kelvin-probe measurement results indicate that the interfacial dipole barriers of Au-pentacene and GR-pentacene are -0.44 and 0.09 eV, respectively. These results can be used to determine the energy alignment levels at the Au-pentacene and GR-pentacene interfaces, as shown in Figure 5. The expected hole-injection barrier heights were then obtained using Equation 2 and were determined to be around 0.54 eV for Au-pentacene and about 0.29 eV for GR-pentacene. The interfacial dipole layer functions unfavorably (that is, it increases the charge-injection barrier) for the Au-pentacene interface, whereas it functions favorably for the GR-pentacene interface. These deduced injection barrier heights are about 20% higher than the effective barrier heights for pentacene OFETs, which were obtained from the temperature-variable I_D - V_D measurements shown in Figure 4. The difference between the barrier height values of the two different types of measurements can be attributed to barrier-lowering effects of transport charges in pentacene OFETs, such as image potential lowering and rounding-off of the barrier corners.^[40–42] Nevertheless, the results of the Kelvin-probe measurements qualitatively confirm that the favorably oriented interfacial dipole layer is the reason for the enhanced performance of graphene electrodes in pentacene OFET devices.

In summary, we have reported that the performance of pentacene OFETs was significantly improved by using multilayer graphene electrodes instead of traditional Au electrodes. Through detailed characterizations of the graphene and pentacene interface, key parameters such as the contact resistance and the charge-injection barrier height were determined. The formation of a favorable interfacial dipole layer at the graphene-pentacene interface was shown to be the main reason for the improved performance of pentacene OFETs with graphene electrodes.

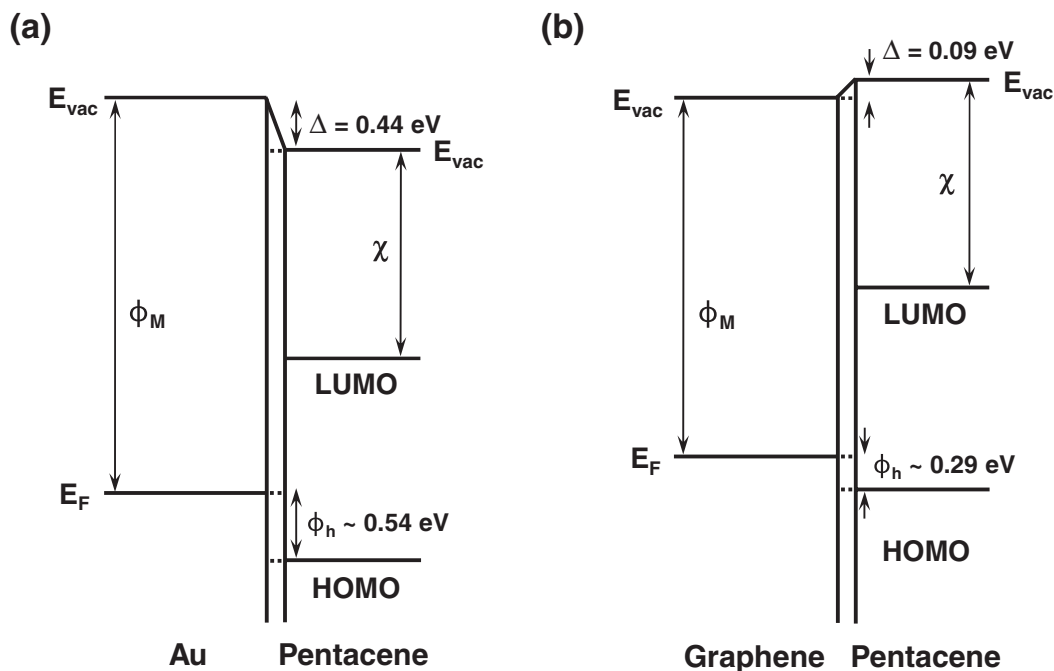


Figure 5. Schematic energy diagrams of a) the Au-pentacene and b) the GR-pentacene interfaces. The energy level alignments with the interfacial dipole barrier were determined by Kelvin-probe measurements. The hole-injection barrier (Φ_h), the electron affinity (χ), and the interfacial dipole barrier (Δ) are indicated in the diagrams.

Experimental Section

The MLG film was synthesized by chemical vapor deposition. First, 300 nm-thick Ni-coated substrates (2 cm \times 2 cm or more in size) were loaded into a quartz tube and pre-annealed at 300 °C under the flow of 200 sccm of Ar mixed with 4% H₂ for 30 min. Subsequently, the temperature of the Ni substrate was raised and the MLG film was grown at 900 °C by flowing 5 sccm of methane and 150 sccm of 4% H₂ in an Ar mixture simultaneously for 5 min. After the growth, the Ni substrate with grown MLG film was rapidly cooled down in order to suppress thick film formation. The synthesized MLG films were transferred and applied as the electrodes of pentacene OFETs using the process described above. The electrical properties of the fabricated OFETs were characterized using a Keithley 4200-SCS parameter analyzer connected to a probe station inside a N₂-filled glove box. To measure the I_D - V_D characteristics with varying temperature, the fabricated devices were loaded into a cryostat (ST-100 from Janis Co.). While the temperature was varied from 300 to 180 K by flowing liquid nitrogen into the sample holder in the vacuum chamber, the I_D - V_D curves were measured at 10 K intervals using a HP4155A semiconductor parameter analyzer.

Supporting Information

Supporting Information is available from the Wiley Online Library or from the author.

Acknowledgements

The authors thank the National Research Laboratory Program, the National Core Research Center grant, the World Class University program by the Korean Ministry of Education, Science and Technology, and the Program of Integrated Molecular Systems at GIST.

Received: August 31, 2010

Published online: November 10, 2010

- [1] S. R. Forrest, *Nature* **2004**, *428*, 911.
- [2] T.-W. Lee, Y. Byun, B.-W. Koo, I.-N. Kang, Y.-Y. Lyu, C. H. Lee, L. Pu, S. Y. Lee, *Adv. Mater.* **2005**, *17*, 2180.
- [3] E. Artukovic, M. Kaempgen, D. S. Hecht, S. Roth, G. Grüner, *Nano Lett.* **2005**, *5*, 757.
- [4] G. Horowitz, *Adv. Mater.* **1998**, *10*, 365.
- [5] Y. Wu, Y. Li, S. Gardner, B. S. Ong, *J. Am. Chem. Soc.* **2005**, *127*, 614.
- [6] H. Yan, Z. Chen, Y. Zheng, C. Newman, J. R. Quinn, F. Dötz, M. Kastler, A. Facchetti, *Nature* **2009**, *457*, 679.
- [7] C. M. Aguirre, C. TERNON, M. Paillet, P. Desjardins, R. Martel, *Nano Lett.* **2009**, *9*, 1457.
- [8] Y. Y. Zhang, Y. Shi, F. Chen, S. G. Mhaisalkar, L.-J. Li, B. S. Ong, Y. Wu, *Appl. Phys. Lett.* **2007**, *91*, 223512.
- [9] M. Lefenfeld, G. Blanchet, J. A. Rogers, *Adv. Mater.* **2003**, *15*, 1188.
- [10] G. Horowitz, *J. Mater. Res.* **2004**, *19*, 1946.
- [11] H. Ishii, K. Sugiyama, E. Ito, K. Seki, *Adv. Mater.* **1999**, *11*, 605.
- [12] A. Kumar, C. Zhou, *ACS Nano* **2010**, *4*, 11.
- [13] L. Diao, C. D. Frisbie, D. D. Schroepfer, P. P. Ruden, *J. Appl. Phys.* **2007**, *101*, 014510.
- [14] F. Amy, C. Chan, A. Kahn, *Org. Electron.* **2005**, *6*, 85.
- [15] C.-G. Lee, S. Park, R. S. Ruoff, A. Dodabalapur, *Appl. Phys. Lett.* **2009**, *95*, 023304.
- [16] C.-a. Di, D. Wei, G. Yu, Y. Liu, Y. Guo, D. Zhu, *Adv. Mater.* **2008**, *20*, 3289.
- [17] S. Pang, H. N. Tsao, X. Feng, K. Müllen, *Adv. Mater.* **2009**, *21*, 3488.
- [18] S. Bae, H. Kim, Y. Lee, X. Xu, J.-S. Park, Y. Zheng, J. Balakrishnan, T. Lei, H. Ri Kim, Y. I. Song, Y.-J. Kim, K. S. Kim, B. Ozyilmaz, J.-H. Ahn, B. H. Hong, S. Iijima, *Nat. Nanotechnol.* **2010**, *5*, 574.
- [19] A. K. Geim, K. S. Novoselov, *Nat. Mater.* **2007**, *6*, 183.
- [20] A. K. Geim, *Science* **2009**, *324*, 1530.
- [21] K. S. Kim, Y. Zhao, H. Jang, S. Y. Lee, J. M. Kim, K. S. Kim, J.-H. Ahn, P. Kim, J.-Y. Choi, B. H. Hong, *Nature* **2009**, *457*, 706.
- [22] A. Reina, X. Jia, J. Ho, D. Nezich, H. Son, V. Bulovic, M. S. Dresselhaus, J. Kong, *Nano Lett.* **2009**, *9*, 30.

- [23] D. Wei, Y. Liu, Y. Wang, H. Zhang, L. Huang, G. Yu, *Nano Lett.* **2009**, *9*, 1752.
- [24] J. Wu, M. Agrawal, H. A. Becerril, Z. Bao, Z. Liu, Y. Chen, P. Peumans, *ACS Nano* **2009**, *4*, 43.
- [25] P. Matyba, H. Yamaguchi, G. Eda, M. Chhowalla, L. Edman, N. D. Robinson, *ACS Nano* **2010**, *4*, 637.
- [26] Y. Wang, X. Chen, Y. Zhong, F. Zhu, K. P. Loh, *Appl. Phys. Lett.* **2009**, *95*, 063302.
- [27] J. Wu, H. A. Becerril, Z. Bao, Z. Liu, Y. Chen, P. Peumans, *Appl. Phys. Lett.* **2008**, *92*, 263302.
- [28] X. Wang, L. Zhi, K. Müllen, *Nano Lett.* **2008**, *8*, 323.
- [29] V. C. Tung, L.-M. Chen, M. J. Allen, J. K. Wassei, K. Nelson, R. B. Kaner, Y. Yang, *Nano Lett.* **2009**, *9*, 1949.
- [30] C. D. Dimitrakopoulos, P. R. L. Malenfant, *Adv. Mater.* **2002**, *14*, 99.
- [31] G. S. Tulevski, C. Nuckolls, A. Afzali, T. O. Graham, C. R. Kagan, *Appl. Phys. Lett.* **2006**, *89*, 183101.
- [32] Y. Lee, S. Bae, H. Jang, S. Jang, S.-E. Zhu, S. H. Sim, Y. I. Song, B. H. Hong, J.-H. Ahn, *Nano Lett.* **2010**, *10*, 490.
- [33] G. Horowitz, P. Lang, M. Mottaghi, H. Aubin, *Adv. Funct. Mater.* **2004**, *14*, 1069.
- [34] G. Jo, J. Maeng, T.-W. Kim, W.-K. Hong, B.-S. Choi, T. Lee, *J. Appl. Phys.* **2007**, *102*, 084508.
- [35] H. Klauk, G. Schmid, W. Radlik, W. Weber, L. Zhou, C. D. Sheraw, J. A. Nichols, T. N. Jackson, *Solid-State Electron.* **2003**, *47*, 297.
- [36] J. Chen, L. C. Calvet, M. A. Reed, D. W. Carr, D. S. Grubisha, D. W. Bennett, *Chem. Phys. Lett.* **1999**, *313*, 741.
- [37] C. Y. Nam, D. Tham, J. E. Fischer, *Nano Lett.* **2005**, *5*, 2029.
- [38] G. Horowitz, P. Delannoy, *J. Appl. Phys.* **1991**, *70*, 469.
- [39] M. Weis, M. Nakao, J. Lin, T. Manaka, M. Iwamoto, *Thin Solid Films* **2009**, *518*, 795.
- [40] D. K. Schroder, *Semiconductor Materials and Device Characterization*, John Wiley & Sons, New York **1998**.
- [41] E. H. Huisman, C. M. Guédon, B. J. van Wees, S. J. Van Der Molen, *Nano Lett.* **2009**, *9*, 3909.
- [42] J. M. Beebe, B. Kim, J. W. Gadzuk, C. Daniel Frisbie, J. G. Kushmerick, *Phys. Rev. Lett.* **2006**, *97*, 026801.